Title

High-temperature neutrino-nucleus processes in stellar collapse

Journal

The Astrophysical Journal, 376(2)

ISSN

0004-637X

Authors

Fuller, George M

Meyer, Bradley S

Publication Date

1991-08-01

DOI

10.1086/170317

Peer reviewed

THE ASTROPHYSICAL JOURNAL, 376:701–716, 1991 August 1

HIGH-TEMPERATURE NEUTRINO-NUCLEUS PROCESSES IN STELLAR COLLAPSE

GEORGE M. FULLER[1,3,4] & BRADLEY S. MEYER[2,3,4]

Received 1991 January 4; accepted 1991 January 31

ABSTRACT

We investigate neutral current neutrino-nucleus interactions of interest in the supernova problem: endothermic and exothermic inelastic neutrino scattering processes; de-excitation of hot nuclei into neutrino pairs; and neutrino-antineutrino annihilation processes involving nuclei. We employ a shell model based treatment including allowed and forbidden transitions to compute the relevant weak strength distributions in nuclei. We discuss Fermi gas fitting formulae for the differential cross sections of all four processes for use in numerical stellar collapse calculations. Since target nuclei in stellar collapse are expected to be in highly excited states we explicitly include thermal effects in our calculations. We find that low-energy neutrino-pair production from hot nuclei and exothermic neutrino-nucleus scattering may have an important role in determining the evolution of the lepton distribution functions in the infalling presupernova core.

Subject headings: neutrinos — nuclear reactions — stars: collapsed — stars: supernovae

1. INTRODUCTION

In this paper we re-examine and extend the results of the pioneering survey on the production and scattering of neutrinos by nuclei at high temperatures in stellar collapse done by Kolb & Mazurek (1979). Haxton (1988b, also Woosley et al. 1990) has revived interest in this subject by performing detailed shell model calculations of inelastic neutrino-nucleus scattering rates in the endothermic channel (where the neutrino scatters to a lower energy state). He has shown that giant-resonance forbidden-weak nuclear transitions can make important, even dominant, contributions to these rates when neutrino energies are large enough (~ 10 MeV) to give substantial momentum transfer to nuclei. With this forbidden strength Haxton's (1988b) scattering rates can be one order of magnitude larger than those predicted in Kolb & Mazurek (1979). Subsequently Bruenn & Haxton (1989, 1991) have shown that this enhanced rate of neutrino down-scattering (to lower energy) could lead to significant modification of the lepton number distribution physics in the pre-supernova core which, in turn, could have an effect on the initial shock energy.

In light of these developments it is important to extend a similar shell model treatment to the other neutrino-nucleus interactions, both because the rates of these processes may be different than previously calculated and because they may tend to compensate the effects of endothermic neutrino-nucleus scattering in the collapse. To this end we extend the calculations of Haxton (1988b) to finite temperature and to three additional closely related neutrino-nucleus interaction processes.

The processes which we consider are shown in Figures 1*a*–1*d*: two endothermic processes where neutrinos transfer energy to nuclei, including inelastic scattering and the three-body process of neutrino pair annihilation on nuclei; and two exothermic processes where nuclei in thermally excited states transfer energy to neutrinos, including exothermic inelastic scattering and de-excitation of nuclear excited states into neutrino pairs. All of these processes are closely related in their nuclear physics properties but substantial differences exist in regards to neutrino phase-space considerations.

In § 2 we will briefly consider the relevant matrix elements and phase-space factors for the four neutrino-nucleus processes. The nuclear shell model calculations for the weak strength distributions are described in § 3. Simple Fermi gas motivated fitting formulae are derived in § 4 and applied to our shell model results from § 3. We discuss the expected angular distribution for neutrino scattering in § 5. The effects of neutrino-nucleus processes on the temperature, lepton fraction, and entropy in the collapsing stellar core are discussed in § 6. One zone collapse calculations are presented which illustrate the relative importance of the neutrino-nucleus processes in stellar core collapse and the supernova problem.

2. THE FUNDAMENTAL PROCESSES

In what follows we assume weak interaction universality for ν_e, ν_μ, and ν_τ interactions. The effective Lagrangian for weak neutral current interactions is taken to be

$$\mathscr{L} = \frac{G}{\sqrt{2}} \bar{\nu}\gamma_\mu(1 - \gamma_5)\nu J_Z^\mu , \tag{2.1}$$

where G is the weak coupling constant, $\nu(\bar{\nu})$ are neutrino spinors, and J_Z^μ is the nuclear (hadronic) neutral weak current which we take to be

$$J_Z^\mu = \bar{\Psi}_f[C_V \gamma^\mu - C_A \gamma^\mu \gamma_5]\Psi_i . \tag{2.2}$$

[1] Postal address: Physics Department 0319, University of California, San Diego, La Jolla, CA 92093-0319.
[2] Postal address: Department of Physics and Astronomy, Clemson University, Clemson, SC 29634.
[3] Institute of Geophysics and Planetary Physics, University of California, Lawrence Livermore National Laboratory, Livermore, CA 94550.
[4] Institute for Nuclear Theory, University of Washington, Seattle, WA 98195.

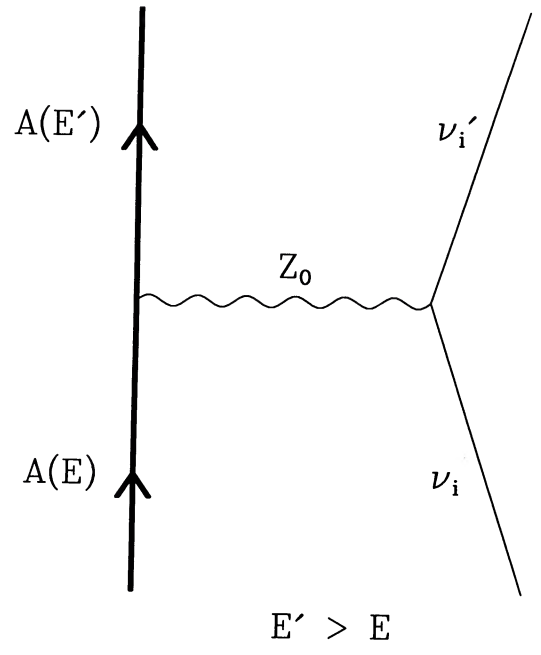

FIG. 1*a*

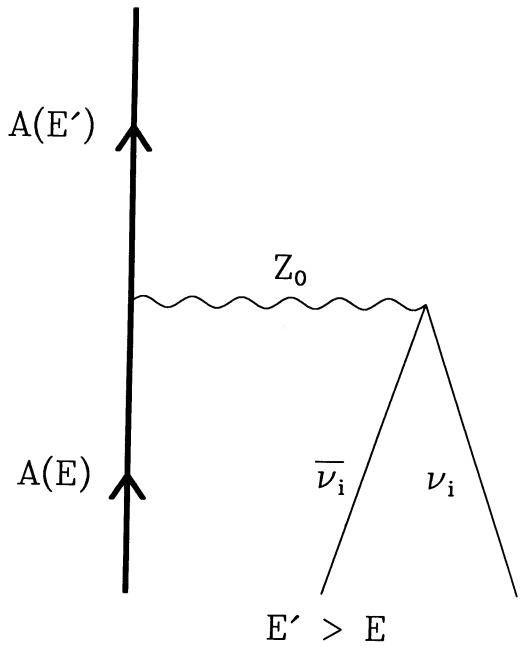

FIG. 1*b*

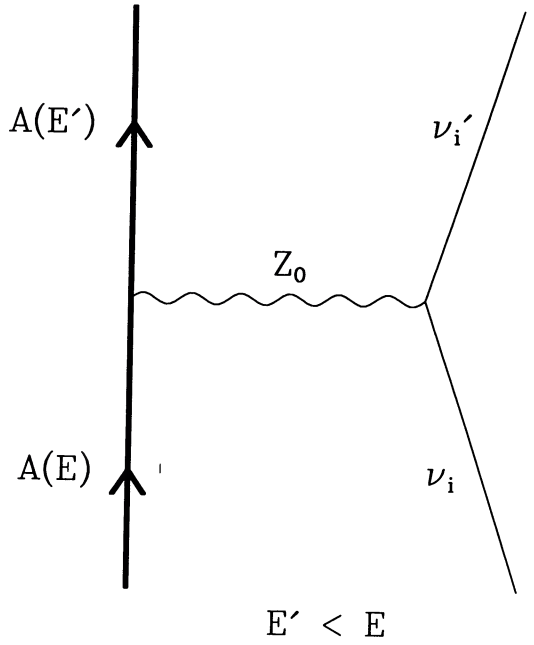

FIG. 1*c*

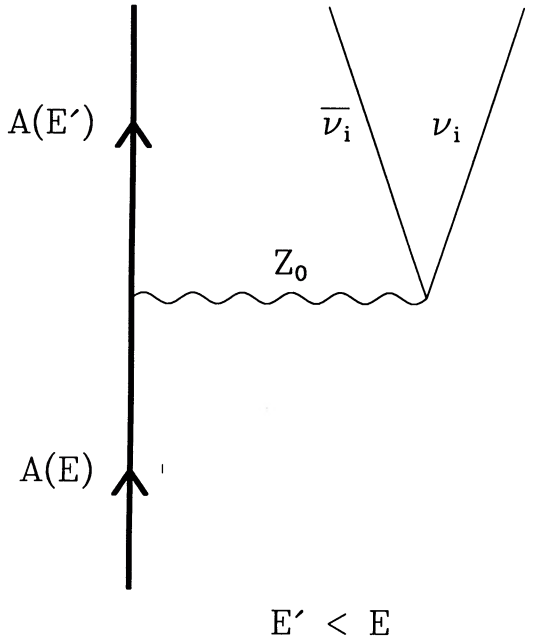

FIG. 1*d*

FIG. 1.—Four neutral neutrino-nucleus interaction processes are shown. In each case neutrinos of flavor i (here i can be e, μ, or τ) interact with a nucleus of A nucleons. The initial and final excitation energies of the nucleus are E and E', respectively. The processes are (*a*) endothermic scattering, (*b*) neutrino pair annihilation, (*c*) exothermic inelastic scattering, and (*d*) thermal de-excitation into neutrino pairs.

In this expression Ψ_i and Ψ_f represent initial and final nuclear spinors and we take C_V and C_A to be *effective* vector and axial vector "form factors" which include dependence on the isospin and on the Weinberg and Cabibbo angles. Strictly speaking C_V and C_A each have both isoscalar and isovector components, but in what follows we will ignore isospin effects and treat the matrix elements as free parameters. These parameters are then fit to the detailed shell model results reported in Woosley et al. (1990) in a manner to be described below.

At the temperatures and densities characteristic of stellar collapse, nucleons are nonrelativistic. If additionally the momentum transfer to the nucleus were small then the nuclear matrix element could be reduced to the familiar allowed, dipole form for M1 (Gamow-Teller) and Fermi transitions,

$$|M_F|^2 = |<\psi_f|C_V\tau_\pm|\psi_i>|^2 \tag{2.3a}$$

and

$$|M_{GT}|^2 = |<\psi_f|C_A\boldsymbol{\sigma}\tau_3|\psi_i>|^2 , \tag{2.3b}$$

where ψ_i and ψ_f are appropriate nuclear wavefunctions derived from the large components of the nuclear spinors and $\boldsymbol{\sigma}$ and $\boldsymbol{\tau}$ are the Pauli spin and isospin operators. In this nonrelativistic limit, of course, there is typically no Fermi strength. The selection rules for Gamow-Teller transitions are $|\Delta J| = 0, \pm 1, \Delta\pi =$ no, and no orbital angular momentum change.

As discussed above it is not sufficient to include only allowed nuclear transitions, as momentum transfer in neutrino-nucleus interactions can be large. We therefore generalize the nuclear matrix element in equation (2.3b) to include first forbidden strength as well as allowed axial-vector strength. All single particle transitions in the nucleus are then assigned the same matrix-element kernel, $|M_{s.p.}|^2$. Considerations of subshell occupation numbers and orders of forbiddenness are taken into account as explained in § 3.

The distribution of single-particle weak strength with nuclear excitation energy is denoted $\beta(E, E' - E)$, where E and E' are the excitation energies of the initial and final nuclear states, respectively. This function is determined from the shell model in the next section. Ultimately we wish to use this strength function to compute double–energy-differential neutrino scattering and production/destruction rates for use in stellar collapse codes. However it is useful to consider first the total scattering rate for one process, which we will take to be endothermic scattering. This discussion will then be illustrative of how we break down the phase space factors for each process into simple kernels from which it is easy to read off the double-energy-(flux)-differential quantities desired.

The total endothermic neutrino scattering rate, integrated over initial neutrino flux and summed over final neutrino phase space is

$$\lambda_{\rm endo} = \sigma_0 \int_0^\infty dE_\nu \mathscr{F}_\nu(E_\nu) \int_0^{E_\nu} dE'_\nu E'^2_\nu (1 - f'_\nu) \left\{ \frac{1}{Z} \int_0^\infty dE \rho(E) e^{-E/kT} \int_E^{E+(E_\nu - E_{\nu'})} dE' \beta(E, E' - E) \delta[E_\nu - E'_\nu - (E' - E)] \right\} , \tag{2.4a}$$

where E_ν and E'_ν are the incident and scattered neutrino energies, respectively, E and E' are the initial and final nuclear energies, respectively, $\mathscr{F}_\nu$ is the incident flux for neutrinos with energies E_ν to $E_\nu + dE_\nu$, f'_ν is the neutrino distribution function in the star evaluated at E'_ν, T is the temperature with k Boltzmann's constant, and δ represents a Dirac delta function. In equation (2.4a) the overall cross-section scale factor is defined

$$\sigma_0 \equiv \frac{G_F^2}{\pi} g_A^2 \approx 6.658 \times 10^{-23} \text{ MeV}^{-4}$$
$$\approx 2.584 \times 10^{-44} \text{ cm}^2 \text{ MeV}^{-2} , \tag{2.4b}$$

where G_F is the Fermi constant (we neglect the small correction for the Cabibo angle, given the nature of our matrix element fits) and $g_A \approx 1.24$ is the ratio of axial-vector-to-vector coupling constants. In these expressions $\rho(E)$ is the nuclear level density and Z is the high temperature nuclear partition function,

$$Z = \int_0^\infty dE \rho(E) e^{-E/kT} . \tag{2.5}$$

As discussed in § 3 we can replace the explicit thermal average in equation (2.4a) with a mean nuclear state, the "representative configuration." This procedure is a good approximation so long as the nuclear mass is large and the temperature is comparable to or larger than the mean single particle level spacing (both of these conditions are met during stellar core collapse). In this limit the average nuclear excitation energy is $\langle E \rangle \approx a(kT)^2$ where a is the level density parameter and is equal to $\sim A/8$ MeV^{-1} where A is the nuclear mass. In terms of this representative configuration and average excitation energy equation (2.4a) reduces to

$$\lambda_{\rm endo} \approx \sigma_0 \int_0^\infty dE_\nu \mathscr{F}_\nu(E_\nu) \int_0^{E_\nu} dE'_\nu (1 - f'_\nu) E'^2_\nu \beta(\langle E \rangle, E_\nu - E'_\nu) ; \tag{2.6}$$

the integrand of which obviously gives the double-energy/flux-differential scattering rate kernel. In like manner we can write the total rate for exothermic scattering as

$$\lambda_{\rm exo} \approx \sigma_0 \int_0^\infty dE_\nu \mathscr{F}_\nu(E_\nu) \int_{\langle E \rangle}^{E_\nu + \langle E \rangle} dE'_\nu E'^2_\nu (1 - f'_\nu) \beta(\langle E \rangle, E'_\nu - E_\nu) , \tag{2.7}$$

where the notation is as above. Again it is obvious that the integrand represents the desired scattering kernel.

We can write the total nuclear de-excitation rate into neutrino pairs in terms of the representative configuration energy $\langle E \rangle$ as

$$\lambda_{\rm de-ex} \approx \lambda_0 \int_0^{\langle E \rangle} dE_\nu E_\nu^2 (1 - f_\nu) \int_0^{\langle E \rangle - E_\nu} dE_{\bar\nu} E_{\bar\nu}^2 (1 - f_{\bar\nu}) \beta(\langle E \rangle, E_\nu + E_{\bar\nu}) , \tag{2.8a}$$

where E_ν and $E_{\bar\nu}$ are the energies of the neutrino and anti-neutrino, respectively, and f_ν and $f_{\bar\nu}$ are the neutrino and anti-neutrino distribution functions, respectively. The overall rate scale factor λ_0 is defined

$$\lambda_0 \equiv \left(\frac{G_F^2}{2\pi^3} \right) g_A^2 \approx 5.134 \times 10^{-3} \text{ MeV}^{-5} \text{ s}^{-1}$$
$$\approx 3.334 \times 10^{-88} \text{ MeV s cm}^4 . \tag{2.8b}$$

In a similar fashion the total neutrino-anti-neutrino annihilation rate on nuclei is

$$\lambda_{\rm ann} \approx \lambda_0 \int_0^\infty dE_\nu \mathscr{F}_\nu \int_0^\infty dE_{\bar\nu} \mathscr{F}_{\bar\nu}(E_{\bar\nu}) \beta(\langle E\rangle, E_\nu + E_{\bar\nu}) , \tag{2.9}$$

where $\mathscr{F}_\nu(E_\nu)[\mathscr{F}_{\bar\nu}(E_{\bar\nu})]$ is the neutrino (anti-neutrino) flux at energy $E_\nu(E_{\bar\nu})$. The desired double-energy(flux)-differential production (annihilation) rates are given by the integrand in equation (2.8a) (eq. [2.9]).

3. THE SHELL MODEL

In order to make estimates of the rates of neutrino-nucleus interactions, we employ an independent single-particle shell model (ISPSM). In this model neutrinos interact with single nucleons in the nucleus. The nucleons are treated as independent particles moving in an average potential; therefore, the resulting energy gain or loss by the nucleus in neutrino-nucleus processes is simply the difference between the initial and final single-particle energies of the relevant nucleon. This model neglects the effects of a residual interaction and configuration mixing. The results in the next section for inelastic neutrino scattering on ground state nuclei compare well with detailed shell model calculations, however. We therefore expect that the independent single-particle shell model adequately describes the essential features of neutrino-nucleus interactions.

As outlined above, it is necessary to include some measure of the forbidden strength in the calculation of neutrino-nucleus interaction rates. This may be done by noting that the degree of forbiddenness in a weak interaction is given by the $i\mathbf{k}\cdot\mathbf{r}$ term in the plane wave expansion of the leptonic current, where $\mathbf{k}$ is the momentum transfer and $\mathbf{r}$ is the coordinate vector. The other variety of forbidden weak current, due to the small components in the nucleon spinors, can be neglected in most supernova conditions (Fuller 1982). Therefore, first forbidden transitions in neutrino-nucleus processes will have rates proportional to $(kR)^2$, where R is the nuclear radius. Other forbidden transitions will have rates proportional to higher powers of (kR).

The total strength for a neutrino-nucleus interaction of energy ΔE in the ISPSM is then the sum of all allowed and forbidden single particle transitions which give energy ΔE. Thus, following Fuller, Fowler, & Newman (1982) the strength β for an transition of energy E from an initial state of excitation energy E is

$$\beta(E, \Delta E) = \sum_{\substack{\text{protons}\\ \text{neutrons}}} \sum_{\substack{i,f\\ \{\Delta E\}}} |M_{if}|^2 \approx |\bar M|^2 \sum_{\substack{\text{protons}\\ \text{neutrons}}} \sum_{\substack{i,f\\ \{\Delta E\}}} \frac{n_i^p n_f^h}{(2j_f+1)} (kR)^N , \tag{3.1}$$

where the sum is over neutrons and protons for all initial single particle levels i and all final single particle levels f, and $|M_{if}|^2$ is the weak matrix element (allowed or forbidden) connecting level i with level f. We approximate $|M_{if}|^2$ as an overall characteristic matrix element $|\bar M|^2$ (to be fit to the detailed shell model calculations of Woosley et al. 1989) times the product of the occupation number of the initial level i, n_i^p, and the fractional number of open holes in the final level f, $n_f^h/(2j_f+1)$. The term $\{E\}$ means that only single particle transitions yielding energy ΔE are included in the sum. In keeping with the independent single-particle shell model, this energy ΔE is

$$\Delta E = |E_f - E_i| , \tag{3.2}$$

where E_i and E_f are the initial and final single particle energies, respectively. For the forbiddenness term $(kR)^N$ in equation (3.1), we take

$$N = 2(|\Delta n| + |\Delta l|) , \tag{3.3}$$

with $|\Delta n| = |n_f - n_i|$ the change in radial quantum number in the single particle transition and $|\Delta l| = |l_f - l_i|$ the change in the orbital quantum number. We exclude all transitions with $N > 2$, however, and thus consider only allowed and first forbidden transitions. We note that, strictly speaking, forbidden transitions would introduce an extra energy dependence in the phase-space integrals in equations (2.4a) through (2.9). In the interest of obtaining a simple fit to the fundamental rates we have neglected this extra energy dependence. At the worst this would tend to underestimate the effect of forbidden weak strength, and to compensate we note that we have a somewhat less restrictive set of selection rules than is strictly correct. Ultimately we justify this procedure by our good fits to the detailed calculations of Woosley et al. (1990).

By restricting the sum in equation (3.1) to transitions for which $E_f > E_i$, we confine ourselves to single–particle "up" transitions. These are the transitions occurring in endothermic scattering (Fig. 1*a*) or $\nu\bar\nu$-annihilation (Fig. 1*b*). Single-particle "down" transitions are those for which $E_f < E_i$. These are transitions occurring in exothermic scattering (Fig. 1*c*) or ν-pair de-excitation (Fig. 1*d*). Therefore, in order to calculate the strength for any of these four processes, it is only necessary to know the initial nuclear configuration(s) (i.e., values of n_i^p and n_f^h).

At zero temperature the nucleus is in its ground state. The initial nuclear configuration of nucleus (Z, A) in the ISPSM is then simply obtained by filling up the single particle orbitals with Z protons and $N = A-Z$ neutrons. At finite temperature, however, the problem is considerably more complicated since many nuclear configurations will be thermally populated. Furthermore, the number of populated configurations will increase essentially exponentially with temperature. Kolb & Mazurek (1979) accounted for this by assuming that the weak strength was a function of the energy which was in turn proportional to the total nuclear level density with a cutoff at sum-rule saturation. They obtained the total weak strength at a given energy by summing strengths over different initial configurations weighted by a Boltzmann population factor, and dividing by a partition function. This Fermi-gas approach ignores the single particle shell model nature of the many-body nuclear wavefunction, however, and does not allow for a quantitative means of studying the effects of forbidden strength. A strictly correct shell-model treatment of finite temperature interactions, on the other hand, would be prohibitive since it would be necessary to construct all nuclear configurations that would

exist at finite temperature T. In this paper, we choose to select a representative excited nuclear configuration at T. If this configuration is truly representative in the sense that most excited configurations resemble it, the strength calculated from it alone should give a good indication of the appearance of the true strength calculated from the ensemble of configurations.

In the shell model we have single particle levels of energy ϵ_i with multiplicity $g_i = 2j_i + 1$. Since these particles follow Fermi-Dirac statistics, the logarithm of the grand partition function, or thermodynamic function, for the noninteracting particles is

$$\Omega = \sum_i \Omega_i \,, \tag{3.4}$$

where the sum is over single particle states and where the Ω_i-values are the thermodynamic functions for individual single-particle states:

$$-\beta\Omega_i = g_i \ln [1 + \exp (\alpha - \beta\epsilon_i)] \,, \tag{3.5}$$

where $\beta = 1/kT$, $\alpha = \beta\mu$, and μ is the chemical potential. Given a fixed number of particles (neutrons or protons) $N = \sum_i n_i$ (where n_i is the single-particle occupation number), we may solve for α via

$$N = -\beta \frac{\partial\Omega}{\partial\alpha} = \sum_i \frac{g_i}{\exp (\beta\epsilon_i - \alpha) + 1} \,. \tag{3.6}$$

The mean number of particles in the single particle level with energy ϵ_j is then

$$\langle n_j \rangle = -\frac{\partial\Omega_j}{\partial\mu} = -\frac{1}{\beta}\frac{\partial \ln Z}{\partial\epsilon_j} = \frac{g_j}{\exp (\beta\epsilon_j - \alpha) + 1} \,, \tag{3.7}$$

where Z is the ordinary partition function (eq. [2.5]). Clearly $N = \sum_j \langle n_j \rangle$ when α is chosen according to equation (3.6).

Let us now populate the shell-model single-particle states at finite temperature according to equation (3.7). We do this by letting $n_i^p = \langle n_i \rangle$ and $n_f^h = (2j_f + 1) - \langle n_f \rangle$. Such a thermal distribution of single particle states defines a thermodynamic configuration. Since this configuration is the mean in an ensemble of configurations, it is an appropriate choice to be the representative of the thermal average.

The initial energy of the target nucleus in the representative configuration is the mean energy of the nucleus, which is given by

$$\langle E \rangle = -\frac{1}{\beta}\frac{\partial \ln Z}{\partial\beta} = \sum_i \frac{g_i\epsilon_i}{\exp (\beta\epsilon_i - \alpha) + 1} \,, \tag{3.8}$$

where again Z is the ordinary partition function; hence, $\beta(E, \Delta E)$ is $\beta(\langle E \rangle, \Delta E)$. In what follows, we always compute the strength function at a given temperature by first computing the representative configuration from equation (3.7). Strictly speaking, then, the strength is a function of the temperature and not the energy of the target nucleus. This is advantageous since we merely need to keep track of the temperature, not the initial energy of the nucleus to compute the strength distributions. On the other hand, the rates in equations (2.6)–(2.9) require $\langle E \rangle$ as input. We should thus calculate $\langle E \rangle$ from equation (3.8). In keeping with our simple approach, we choose instead to consider the simple Fermi gas limit of equation (3.8) which gives $\langle E \rangle \approx a(kT)^2$. This limit is valid when kT is comparable to the level spacing in the nucleus, a situation roughly attained in stellar collapse. The value of the level density parameter a is approximately $A/8$ MeV^{-1}, where A is the nuclear mass, but when specific distributions of nuclei are used, it is perhaps preferable to choose the correct value of a for those nuclei (see, for example, Woosley et al. 1978).

Besides the simplicity of this approach, there are two additional advantages. The first is that we can if we desire alter the model to include correlations, such as BCS pairing (Moretto 1972), or subtraction of continuum states (Tubbs & Koonin 1979) by simply adding the appropriate terms to equation (3.5). The second is that the formalism naturally goes over to that for a Fermi gas for $\sum_i g_i \rightarrow 2\int d^3r \int d^3p/(2\pi\hbar)^3$. This allows us to make connections with Fermi gas studies of neutrino-nucleus processes in a particularly straightforward manner.

At this point we may consider the qualitative features of the ISPSM neutrino-nucleus strength as computed from equation (3.1). Figure 2*a* shows the strength for single-particle-up transitions of ^{56}Fe at $T = 1$ MeV. Figure 2*b* shows the strength for the same transitions but with the first forbidden single particle transitions excluded. Clearly the forbidden transitions open up considerably more strength for neutrino-nucleus interactions, especially for high-energy transitions. Figure 2*c* is the same as Figure 2*a* but now for $T = 5$ MeV. Qualitatively, Figures 2*a* and 2*c* are not greatly different. The effect of higher nuclear temperature on the strength distribution is not large since unblocking by nuclear excitation affects only a few single-particle-up transitions. This is to be contrasted with the many up transitions that were unblocked even at $T = 0$ MeV. Unblocking does affect the allowed transitions, however, since these were mostly blocked at $T = 0$ MeV. This is seen in Figure 2*d*, which is the same as Figure 2*b* but for $T = 5$ MeV.

Unblocking is particularly important in single-particle-down transitions. Figure 3*a* gives the strength for single-particle-down transitions (where now E is in fact $-E$) for ^{56}Fe at $T = 1$ MeV. There is much less strength in these transitions than in the single-particle-up transitions in Figure 2*a*. This is because most single-particle-down transitions are blocked since the lower levels are mostly filled. Figure 3*b*, which is the same as Figure 3*a* but with the first forbidden transitions excluded, is not much different from Figure 3*a* since the forbidden transitions, which are mostly blocked, are only really important for large energy change. At $T = 5$ MeV (Fig. 3*c*), many more transitions are unblocked and, consequently, there is much more strength than in the $T = 1$ MeV case. Moreover, forbidden transitions are more important at higher temperature since higher energy transitions are possible. This may be seen by comparing Figure 3*c* with Figure 3*d*, which is the same as Figure 3*c* but with the first forbidden transitions excluded.

In Figures 3*a* and 3*b*, only four allowed transitions are giving any significant contribution to the down strength in ^{56}Fe. These transitions are $1f_{5/2} \rightarrow 1f_{7/2}$ and $2p_{1/2} \rightarrow 2p_{3/2}$, for both neutrons and protons, which are transitions between spin orbit partner

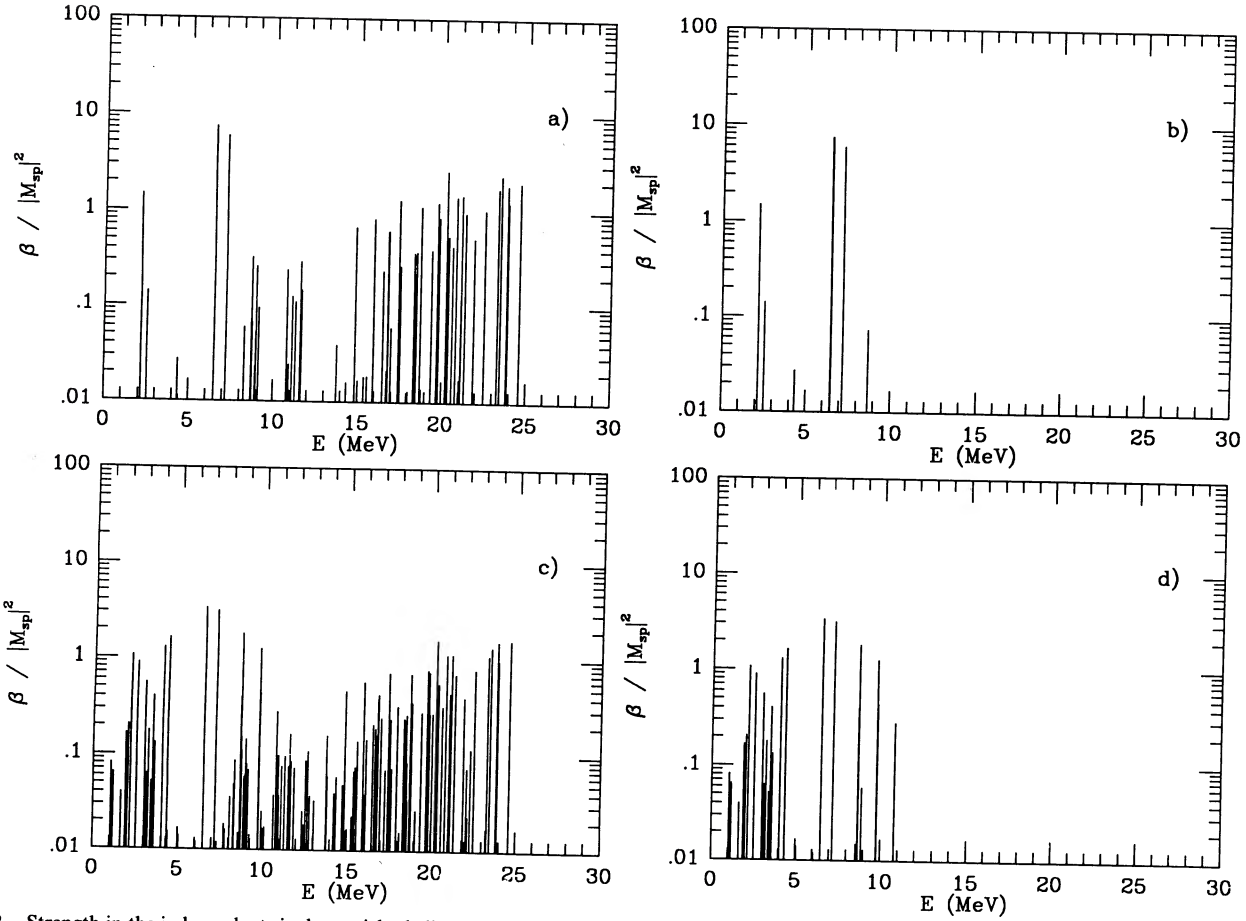

FIG. 2.—Strength in the independent single-particle shell model for up transitions in ^{56}Fe. (*a*) $T = 1$ MeV and allowed and first forbidden transitions. (*b*) $T = 1$ MeV and allowed transitions only. (*c*) Same as Fig. 1*a* but for $T = 5$ MeV. (*d*) Same as Fig. 1*b* but for $T = 5$ MeV.

levels. Similarly in Figures 3*c* and 3*d* transitions between spin orbit partner levels dominate the strength distribution. These results are not surprising, but they are significant. They show that some kind of shell-model treatment is necessary for discovering the true nature of the down strength, namely, that it is dominated by transitions between spin orbit partner levels. As a consequence, the energy scales that arise in this problem are those of the spin orbit splitting in the nuclei under study. We will have more to say about the importance of this observation in § 4.

We can make similar comments about the up strength. The allowed transitions are between spin orbit partner levels. The energies for these transitions lie in the range 1–10 MeV, which is the range of typical spin orbit splitting in the *fp* shell. Forbidden transitions contribute at energies in the range 15–25 MeV where the momentum transfer is large.

For comparison with the detailed shell-model calculations in Woosley et al. (1990) we compute ground-state Fermi-Dirac flux-averaged cross sections for several nuclei with no blocking of the scattered neutrino. In this case,

$$\sigma_{\rm FD}(T) = \frac{\lambda_{\rm endo}}{\int_0^\infty \mathscr{F}_\nu(E_\nu) dE_\nu}, \tag{3.9}$$

where $\lambda_{\rm endo}$ is computed as in equation (2.6a), $\mathscr{F}_\nu(E_\nu)$ is a Fermi-Dirac flux, and $f_{\nu'} = 0$. We fit our results for ^{56}Fe to those of Woosley et al. (1990) by varying $|\bar{M}|^2$. The value for $|\bar{M}|^2$ we found was 0.20. We then use this value for the rest of our calculations.

Figure 4 shows flux-averaged cross sections of ground state configuration nuclei vs. the temperature characterizing the neutrino distribution for (*a*) ^{4}He, (*b*) ^{16}O, (*c*) ^{56}Fe, and (*d*) ^{68}Se. We have good agreement with Woosley et al. (1990) for the heavy nuclei ^{56}Fe (to which we fit) and ^{68}Se. For the lighter nuclei, however, the agreement is not as good. This shows the limitations of our model, due primarily to the lack of the inclusion of configuration mixing in our shell model and to the lack of inclusion of the extra energy dependence in the weak-forbidden transitions. In both the ground state configurations for ^{4}He and ^{16}O in the ISPSM no allowed transitions are possible. Configuration mixing would result in particle-hole excitations which permit allowed single particle transitions to occur in these lighter nuclei. This would result in more strength and larger cross sections, especially at higher temperature. We expect in general, therefore, that neglecting configuration mixing and a residual interaction leads to somewhat underestimated values for the rates of ν-nucleus interactions. Likewise, since forbidden strength clearly dominates the strength for ^{4}He and ^{16}O at zero temperature, not including the extra E^2 factor from forbiddenness in the rate integrands (which is due to the $e^{i\mathbf{k}\cdot\mathbf{r}}$ expansion) leads to an underestimate of the rate. For *sd* and *fp* shell nuclei there are enough allowed transitions that this will not be a problem.

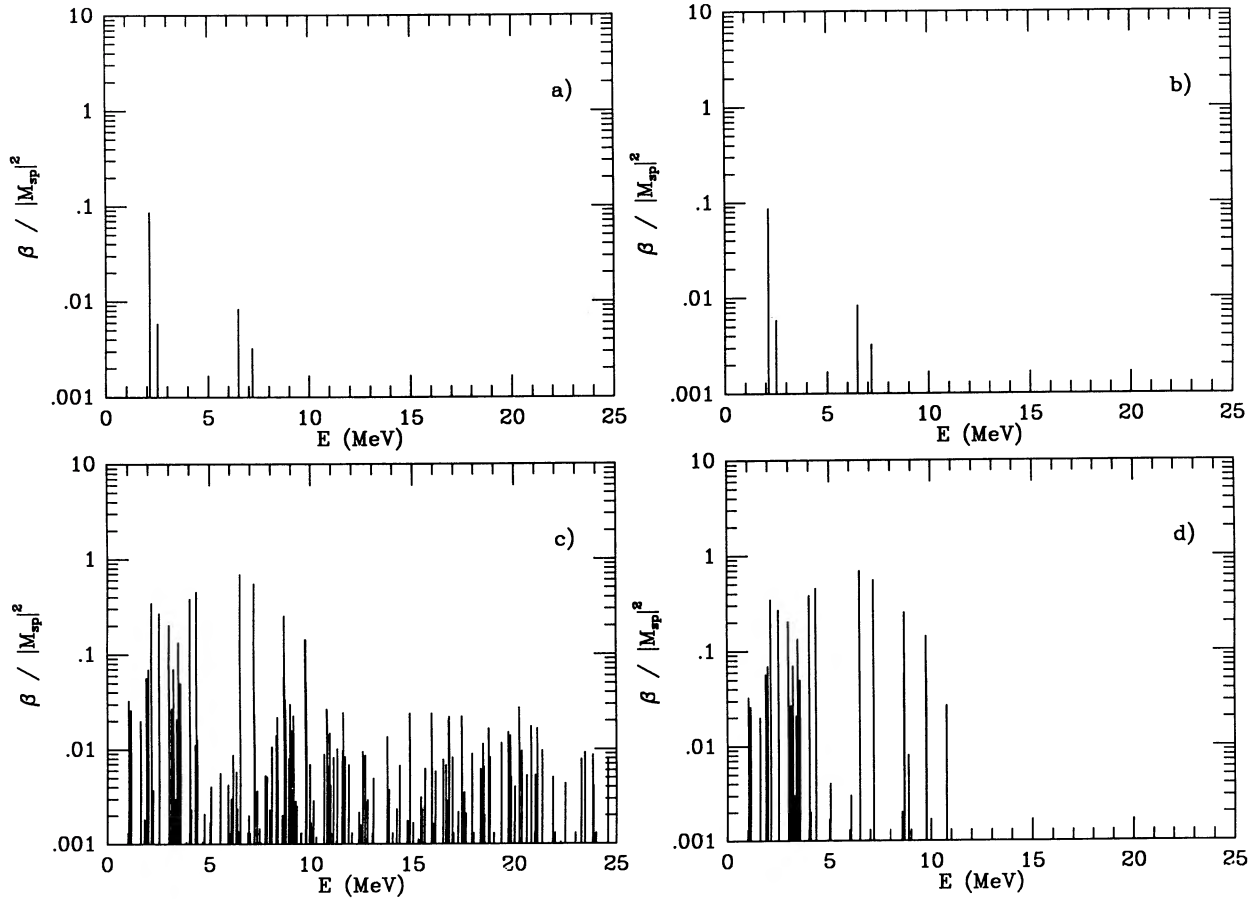

FIG. 3.—Strength in the independent single-particle shell model for down transitions in ^{56}Fe. (*a*) $T = 1$ MeV and allowed and first forbidden transitions. (*b*) $T = 1$ MeV and allowed transitions only. (*c*) Same as Fig. 2*a* but for $T = 5$ MeV. (*d*) Same as Fig. 2*b* but for $T = 5$ MeV.

4. FERMI-GAS-MOTIVATED FITTING FORMULAE

In the previous section we have calculated strength distributions for neutrino-nucleus interactions in the ISPSM. These detailed strength distributions are useful because they show the nature of the variation of strength with temperature and the important underlying single-particle nature of the strength. For example, we have seen that it is the transitions between spin orbit partner levels that dominate the single-particle-down strength. This observation could not have been made in a model that did not consider the details of the shell model nature of the nucleon wavefunctions. The conclusion from a Fermi gas treatment would have been that the dominant contributions to the single-particle-down strength come from transitions of energy kT (Kolb & Mazurek 1979), which is erroneous.

While the ISPSM is useful for clarifying the nature of the strength of neutrino-nucleus interactions, the resulting strength distributions are not useful as input in detailed numerical supernova calculations. Here a Fermi gas treatment is in some ways preferable because, in such a model, the strength functions will simply scale continuously with proton number, neutron number, and temperature. The purpose of this section will be to derive a simple Fermi-gas-based treatment which, however, fits the detailed shell model. Such a scheme will retain the essential energetic and selection rule results of the shell model, yet will be simple to code for all nuclei under a wide range of stellar collapse conditions.

In order to deal with excited nuclei, we continue to work with the representative configuration, which we have taken to be the mean thermodynamic state. In this state the number of initial particle states n_i^p and number of final hole states $n_f^h = g_f - n_f^p$, where again $g = 2j + 1$ is the spin multiplicity of level f, are given by their mean values as computed in equation (3.7). The conversion to the Fermi gas limit is made by replacing the discrete sum $\sum_i g_i$ with the continuous sum $\int 2V\, d^3p_i/(2\pi\hbar)^3$, where V is the nuclear volume. In this limit we find

$$\langle n_i^p \rangle \to \frac{2V\, d^3p_i}{(2\pi\hbar)^3} \frac{1}{e^{(E_i-\mu)/T} + 1} \tag{4.1a}$$

and

$$\frac{\langle n_f^p \rangle}{2j_f + 1} \to 1 - \frac{1}{e^{(E_f-\mu)/T} + 1}, \tag{4.1b}$$

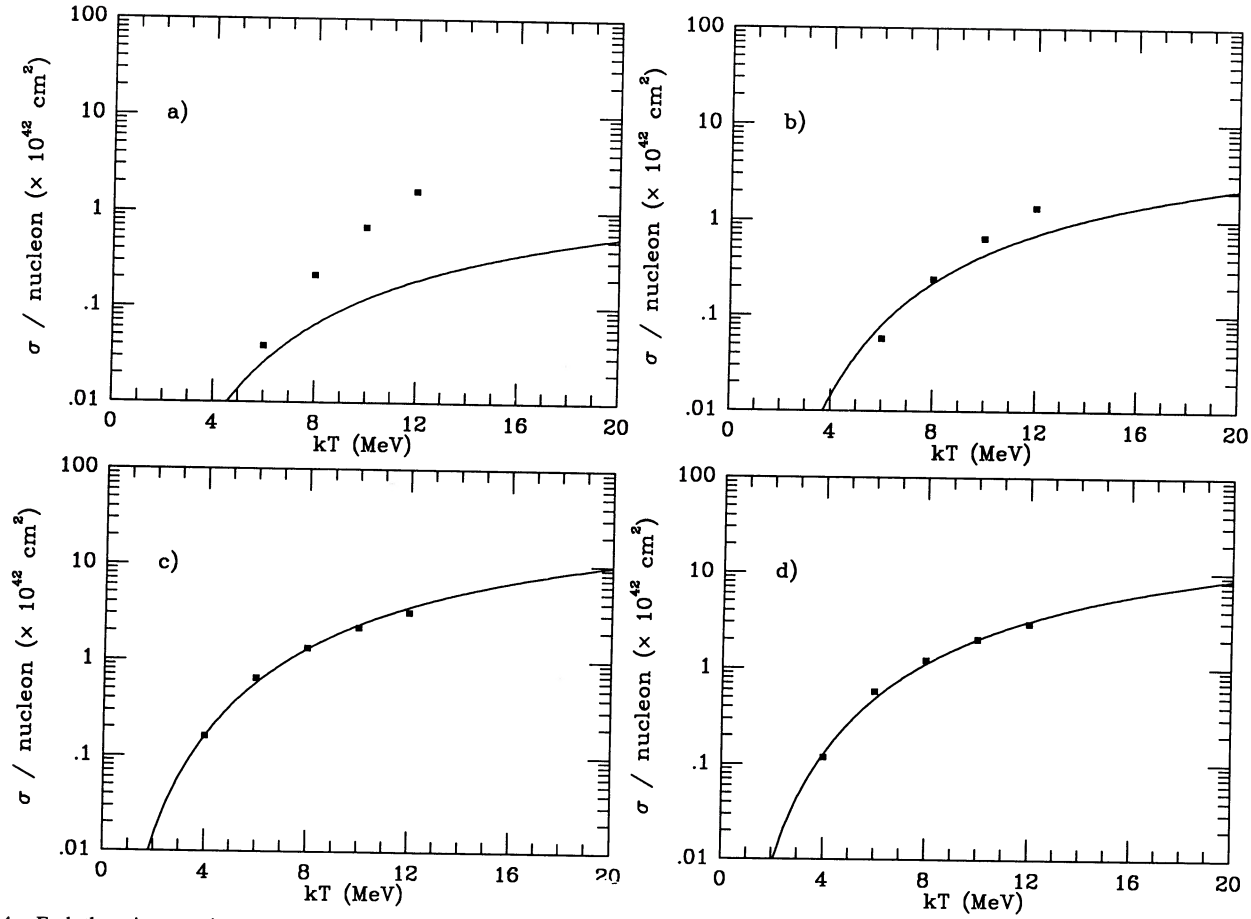

FIG. 4.—Endothermic scattering cross sections averaged over a Fermi-Dirac distribution of neutrinos. Curves are from the ISPSM. Square points are from the detailed shell-model calculations of Woosley et al. 1989 (*a*) ^{4}He, (*b*) ^{16}O, (*c*) ^{56}Fe, and (*d*) ^{68}Se.

where E_i and E_f are the initial and final energies of the single particle making the transition and μ is the nuclear Fermi energy which is of order 40 MeV. We consider here transitions such that $E_f = E_i \pm \Delta E$, where the upper sign refers to endothermic (single-particle-up) transitions and the lower sign refers to exothermic (single-particle-down) transitions. Summation over the final levels will simply pick out the correct energy of the final state for a transition of energy ΔE; thus, by direct substitution into equation (3.1), we find

$$\beta(\langle E\rangle, \Delta E) = \frac{2V}{(2\pi\hbar)^3}\int_0^\infty d^3p_i \frac{1}{e^{(E_i-\mu)/kT}+1}\left(1-\frac{1}{e^{(E_f-\mu)/kT}+1}\right). \tag{4.2}$$

For endothermic (up) transitions, $E_f = E_i + \Delta E$. With this substitution, we can factor the integrand to obtain

$$\beta(\langle E\rangle, \Delta E) = \frac{2V}{(2\pi\hbar)^3}\int_0^\infty d^3p_i \frac{1}{1-e^{-\Delta E/kT}}\left[\frac{1}{1+e^{(E_i-\mu)/kT}}-\frac{1}{e^{[E_i-(\mu-\Delta E)]/kT}+1}\right]. \tag{4.3}$$

If we carry out the integration, we find

$$\beta(\langle E\rangle, \Delta E) = \frac{\sqrt{2}(mc^2)^{3/2}V}{\pi^2(\hbar c)^3}\left[\frac{(kT)^{3/2}}{1-e^{-\Delta E/kT}}\right]\left[F_{1/2}\left(\frac{\mu}{kT}\right)-F_{1/2}\left(\frac{\mu-\Delta E}{kT}\right)\right], \tag{4.4}$$

where $F_{1/2}(\eta)$ is the Fermi integral of order $\frac{1}{2}$ given by

$$F_{1/2}(\eta) = \int_0^\infty \frac{x^{1/2}\,dx}{e^{x-\eta}+1}. \tag{4.5}$$

We note that the nuclear volume is $V = 4\pi r_0^3 A/3$, where $r_0 = 1.2$ fm. In the limit of large nuclear degeneracy ($\mu \gg kT$), which obtains in the region of interest in stellar collapse,

$$\beta(\langle E\rangle, \Delta E) = 79f\left(\frac{A}{60}\right)\left(\frac{\mu}{40\text{ MeV}}\right)^{3/2}\frac{1}{1-e^{-\Delta E/T}}\left[1-\left(1-\frac{\Delta E}{\mu}\right)^{3/2}\right], \tag{4.6}$$

where f has units MeV^{-1} and is to be fit to give the fraction of transitions which are allowed to occur.

The fit in equation (4.6) does not account for any difference between allowed and forbidden strength, nor between neutrons and protons. In order to get better agreement with the ISPSM results of § 3, it is necessary to introduce at least some of the features of the shell model in the Fermi gas treatment. This is done in the following way.

The ISPSM showed us that the allowed transitions resulted from transitions within a given shell between spin orbit partner levels. Forbidden transitions occur predominantly between levels in different shells. This led to allowed transitions mainly in the energy range 1 MeV $< \Delta E <$ 10 MeV. Most of the forbidden strength lies in the energy range 15 MeV $< \Delta E <$ 25 MeV. To this end we consider factors such as $\{1/[e^{(E_1-\Delta E)/\lambda_1}+1]\}\ \{1/[e^{(\Delta E-E_2)/\lambda_2}+1]\}$. Such factors will pick out transitions with $E_1 < \Delta E < E_2$, with the parameters λ determining the strength cutoff. We can then choose separate parameters for allowed and forbidden transitions and can include a $(k \cdot R)^2$ term for the forbidden transitions. Finally, we can treat the protons and neutrons as separate Fermi gasses. This will allow us to fit strength distributions of nuclei with different neutron-to-proton ratios.

With these considerations in mind, we can refine our Fermi gas fit. We obtain for the endothermic (up) strength

$$\beta_{\rm up}(\langle E\rangle, E) = I_0^{\rm up}(\Delta E, T, Z, A)[I_A(\Delta E, \lambda_1, E_1, \lambda_2, E_2) + I_F(\Delta E, \lambda_3, E_3, \lambda_4, E_4)]\ , \tag{4.7a}$$

where the overall Fermi-gas form factor is

$$I_0^{\rm up}(\Delta E, T, Z, N) = 79f\frac{1}{1-e^{-\Delta E/T}}\left\{\left(\frac{Z}{30}\right)\left[1-\left(1-\frac{\Delta E}{\mu_p}\right)^{3/2}\right]+\left(\frac{N}{30}\right)\left[1-\left(1-\frac{\Delta E}{\mu_n}\right)^{3/2}\right]\right\}, \tag{4.7b}$$

the allowed strength form factor is

$$I_A(\Delta E, \lambda_1, E_1, \lambda_2, E_2) = \left(\frac{1}{e^{(E_1-\Delta E)/\lambda_1}+1}\right)\left(\frac{1}{e^{(\Delta E-E_2)/\lambda_2}+1}\right), \tag{4.7c}$$

and the forbidden form factor is

$$I_F(\Delta E, \lambda_3, E_3, \lambda_4, E_4) = \frac{1.4A^2\Delta E^2}{(\hbar c)^2}\left(\frac{1}{e^{(E_3-\Delta E)/\lambda_3}+1}\right)\left(\frac{1}{e^{(\Delta E-E_4)/\lambda_4}+1}\right). \tag{4.7d}$$

In these equations Z and N are the nuclear proton and neutron number, respectively, so that the total nucleon number is $A = Z + N$, and the proton and neutron nuclear Fermi levels are

$$\mu_p = 50\left(\frac{Z}{30}\right)^{2/3}\ , \tag{4.8a}$$

and

$$\mu_n = 50\left(\frac{N}{30}\right)^{2/3}\ . \tag{4.8b}$$

We have left out of our overall Fermi gas form factor the $\mu^{3/2}$ factor, as this will only vary slowly with nuclear mass and temperature. Again, f is an overall fit-parameter related to the ratio of allowed/forbidden transitions in the shell model to those among plane-wave fermions.

Figure 5 shows the binned strength for single-particle-up transitions in various nuclei at temperatures of 1, 2, and 5 MeV as computed in the ISPSM. The curves are the strength distributions computed from equation (4.7). The values of f, E_1, λ_1, etc., used to compute the curves are shown in Table 1. The overall agreement of these curves with the ISPSM results is good. The general features of the strength distribution are well-reproduced, namely the magnitude, spread, and distribution of allowed and forbidden strength. Furthermore, the fits seem to work well for varying temperatures and varying degrees of neutron-richness of the nuclei.

A similar analysis may be made for single-particle-down transitions, for which $E_f = E_i - \Delta E$. In this case the Fermi gas result is

$$\beta(\langle E\rangle, \Delta E) = 79f\left(\frac{A}{60}\right)\left(\frac{\mu}{40\ \text{MeV}}\right)^{3/2}\frac{1}{e^{\Delta E/T}-1}\left[\left(1+\frac{\Delta E}{\mu}\right)^{3/2}-1\right], \tag{4.9}$$

TABLE 1

PARAMETERS FOR USE WITH EQUATION (4.7)

Parameter	Value
f	0.1
E_1	4.0 MeV
λ_1	1.0 MeV
E_2	4.9 MeV
λ_2	1.2 MeV
E_3	17.0 MeV
λ_3	8.0 MeV
E_4	24.0 MeV
λ_4	0.5 MeV

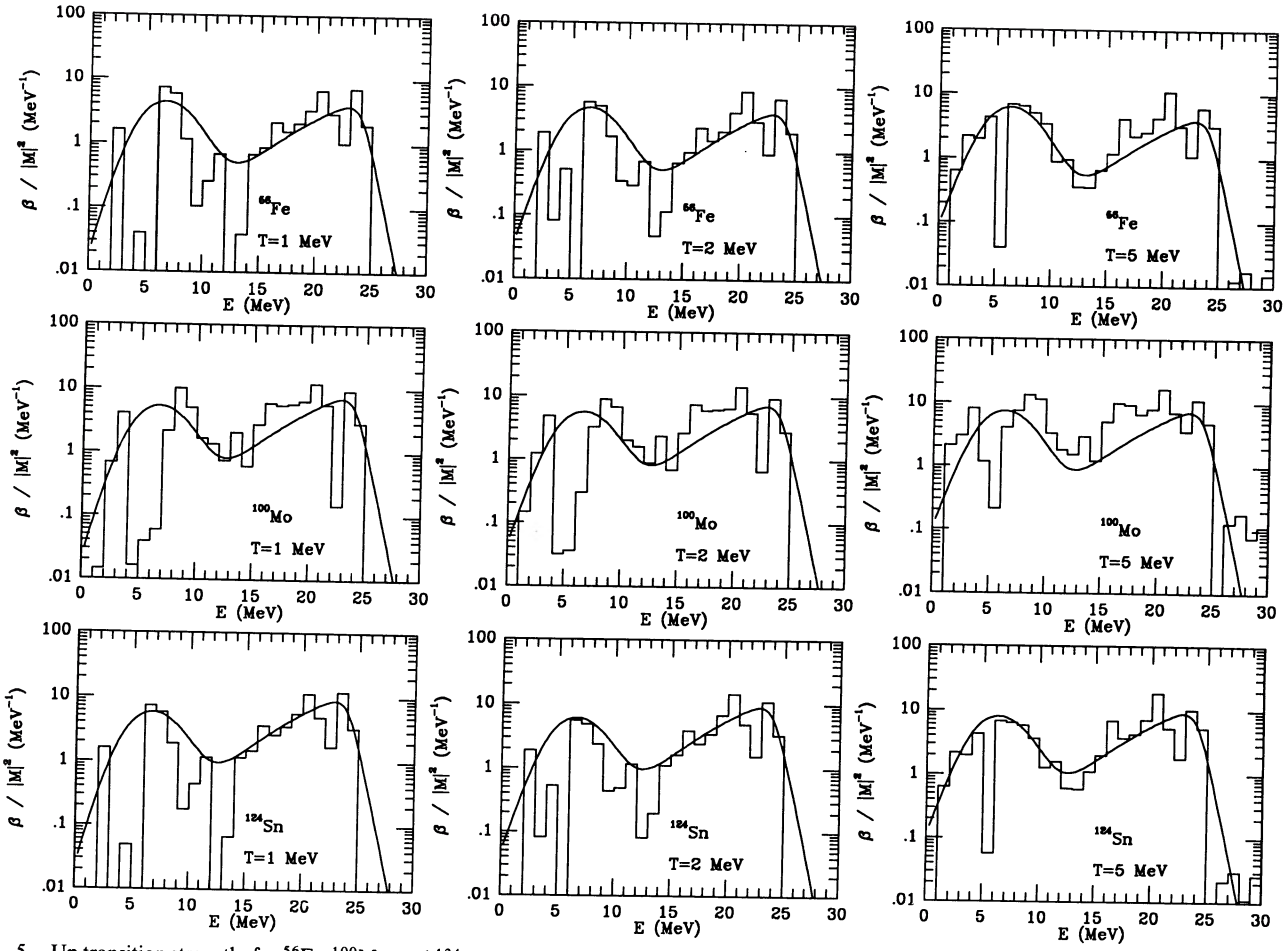

FIG. 5.—Up transition strengths for ^{56}Fe, ^{100}Mo, and ^{124}Sn at temperatures $T = 1$, 2, and 5 MeV. The histograms are binned strength from the ISPSM, while the curves are from the Fermi gas model. The quantity f is the normalization factor for the Fermi gas strength to match the binned strength integrated over energy.

where again f is to be fit. This strength function peaks at $\Delta E = 0$, which disagrees with the ISPSM results. We again pick out allowed and forbidden transitions to get our modified Fermi-gas fit for exothermic transitions:

$$\beta_{\rm down}(\langle E\rangle, \Delta E) = I_0^{\rm down}(\Delta E, T, Z, N)[I_A(\Delta E, \lambda_1, E_1, \lambda_2, E_2) + I_F(\Delta E, \lambda_3, E_3, \lambda_4, E_4)] , \tag{4.10a}$$

where the Fermi-gas form factor is now

$$I_0^{\rm down} = 79f\frac{1}{e^{\Delta E/kT}-1}\left\{\left(\frac{Z}{30}\right)\left[\left(1+\frac{\Delta E}{\mu_p}\right)^{3/2}-1\right]+\left(\frac{N}{30}\right)\left[\left(1+\frac{\Delta E}{\mu_n}\right)^{3/2}-1\right]\right\} , \tag{4.10b}$$

with the notation as before. The allowed, I_A, and forbidden, I_F, form factors are the same as given in equations (4.7c) and (4.7d), except that fitting parameters ($f, \lambda_1, E_1, \lambda_2, E_2, \lambda_3, E_3, \lambda_4, E_4$) differ for the down transitions and are given in Table 2.

TABLE 2

PARAMETERS FOR USE WITH EQUATION (4.10)

Parameter	Value
f	$0.09 + 0.017T^2$
E_1	3.0 MeV
λ_1	1.0 MeV
E_2	4.0 MeV
λ_2	1.0 MeV
E_3	17.0 MeV
λ_3	8.0 MeV
E_4	22.0 MeV
λ_4	1.0 MeV

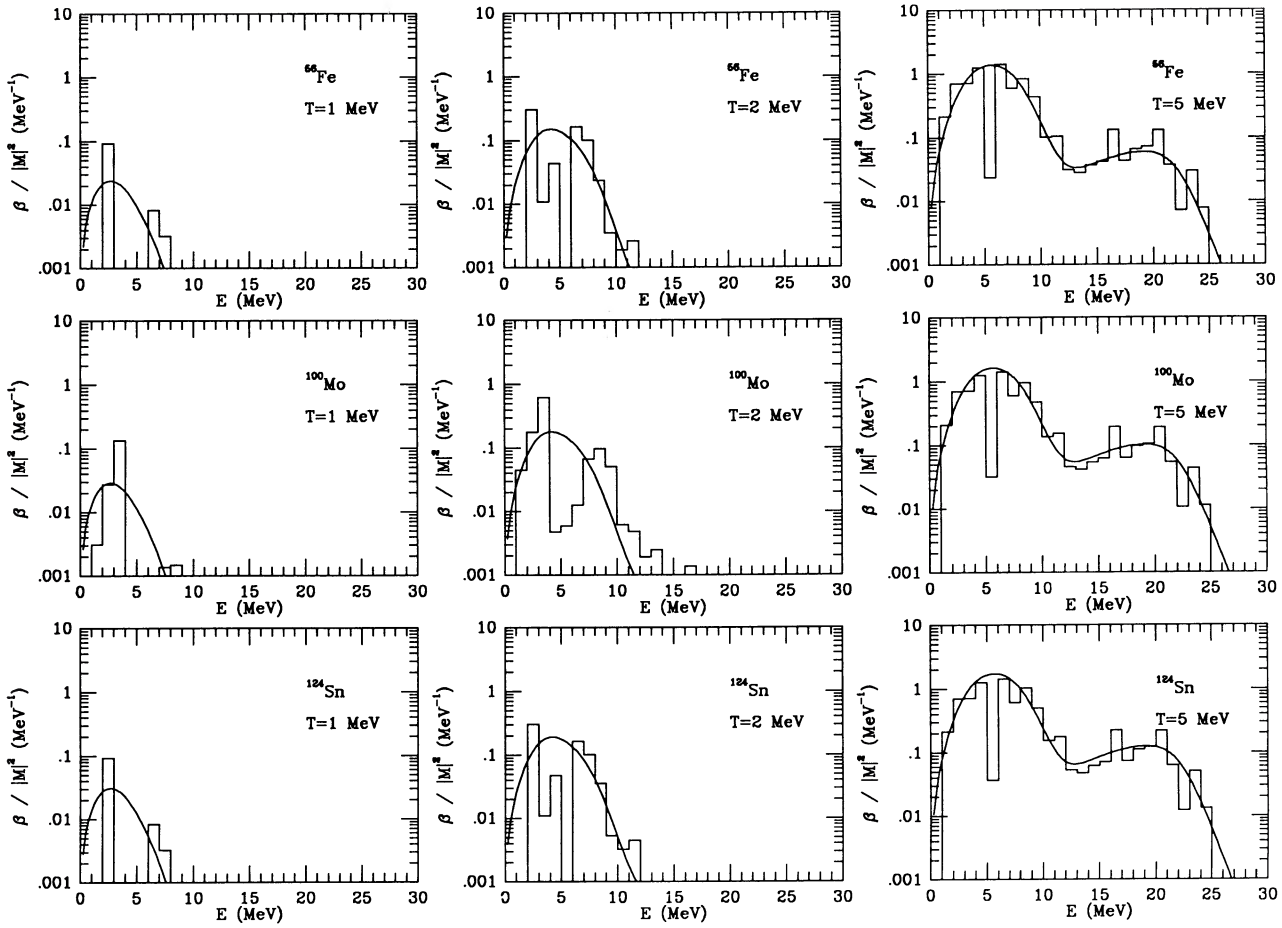

FIG. 6.—Down transition strengths for the indicated nuclei. The histograms are binned strength from the ISPSM, while the curves are from the Fermi gas model. The quantity f is the normalization factor for the Fermi gas strength to match the binned strength integrated over energy.

Figure 6 corresponds to Figure 5 but is for single-particle down transitions. Curves show the fit of equation (4.10). The values of f, E_1, λ_1, etc., used for these curves are shown in Table 2. Again the agreement between the ISPSM results and the modified Fermi-gas results are good over a range of nuclear masses and temperatures.

In summary, we have computed the strength distributions for neutrino-nucleus interactions in the Fermi gas limit. We have modified the results to obtain better agreement with results from the ISPSM by taking allowed and forbidden transitions to fall in different energy ranges. The fits made on the basis of the modified Fermi-gas results agree well with the ISPSM results. Equation (4.7), with the fitting parameters in Table 1, may be used for the strength distribution in endothermic processes (Figs. 1*a* and 1*b*; eqs. [2.6] and [2.9]), while equation (4.10), with the parameters in Table 2 may be used for the strength distribution in exothermic processes (Figs. 1*c* and 1*d*; eqs. [2.7] and [2.8]).

5. ANGULAR DISTRIBUTIONS

It may be necessary to know the angular distribution of the neutrinos in ν-nucleus interactions. The angular distributions of the electron and antineutrino emitted in β-decay are given in detail in Greuling & Meekes (1951) and Morita (1953). To the extent that isospin is a good quantum number in nuclei, a reasonable approximation in our model, these distributions apply to ν-nucleus interactions as well.

All of our allowed strength comes from Gamow-Teller transitions. The angular distribution is

$$P(\Omega) = \frac{1}{4\pi}\left(1 - \frac{1}{3}\cos\theta\right), \tag{5.1}$$

where θ is the angle between the momenta of the neutrinos in the entrance and exit channels and $P(\Omega)$ is normalized for integration over $d\Omega = \sin\theta\, d\theta\, d\phi$. This distribution is slightly backward peaked. Note that for $\nu\bar{\nu}$-emission and annihilation one may view the antineutrino as a neutrino moving backwards in time; therefore, it is in the entrance channel in emission and the exit channel for annihilation.

The angular distribution for forbidden transitions is a complicated matter. In first forbidden β-decay (or charged-current ν-nucleus interactions) where Coulomb wave corrections are important in the energetics of the emitted electron, the angular

distribution depends strongly on the nature of the interaction. A vector interaction will tend to have a distribution that goes roughly as $1 + \cos\theta$, which is strongly forward peaked. An axial-vector interaction will tend to be strongly backward-peaked ($1 - \cos\theta$). Haxton (1987) finds charged-current capture on ^{16}O to be strongly backward-peaked. Because ^{16}O has a total isospin quantum number $T = 0$ ground state and little allowed strength, charged-current interactions to ^{16}N or ^{16}F (both $T = 1$ in the ground state) will proceed primarily through forbidden axial-vector transitions. These transitions favor large momentum transfer to the nucleus and, consequently, relatively low-energy (compared to the incident neutrino energy) for the emitted electron. The angular distribution then is backward peaked.

For neutral-current interactions the exit channel lepton is neutral; therefore, Coulomb wave-correction terms in the angular distribution are irrelevant. As above, however, the angular distribution will depend strongly on which operators in the weak Hamiltonian contribute most to the overall forbidden strength. For example, the vector operator $\boldsymbol{r}$ gives a matrix element $|\boldsymbol{r}|^2$ proportional to roughly $1 + \cos\theta$. The axial vector operator $\boldsymbol{\sigma} \times \boldsymbol{r}$ has a square matrix element $|\boldsymbol{\sigma} \times \boldsymbol{r}|^2$ roughly proportional to $1 - \cos^2\theta$, which is peaked at $\theta = \pi/2$. The vector operator $\boldsymbol{\sigma}$ has a square matrix element $|\boldsymbol{\sigma}|^2$ proportional to $1 - \frac{1}{3}\cos\theta$, which is slightly backward peaked. There also are terms that are essentially isotropic. Although many terms appear to be roughly forward peaked for first-forbidden decay, we do not have sufficient detail in our model to determine the magnitude of the various terms and their relative contribution to the overall angular distribution. We assume for now that the angular distribution for the forbidden transitions is roughly isotropic because we have terms that peak at $\theta = 0, \pi/2$, and π. Thus,

$$P_F(\Omega) \approx \frac{1}{4\pi} . \tag{5.2}$$

If certain operators are found to dominate the forbidden strength for ν-nucleus interactions, we can alter $P(\Omega)$ accordingly. We do not expect, however, that forbidden transitions will play a dominant role in ν-nucleus interactions in the heavier mass nuclei relevant for stellar collapse. As we have seen, down transition strength is completely dominated by allowed transitions. Because phase space considerations favor large exit channel neutrino energy and, hence, low momentum transfer to nuclei, allowed transitions will also completely dominate up transitions (endothermic processes) when significant allowed strength is available. Such allowed strength is available to almost all nuclei present in a collapsing star. Our ignorance of the exact form for $P_F(\Omega)$ should therefore have little effect on calculations of the overall angular distribution for ν-nucleus processes in stellar collapse.

With $P_A(\Omega)$ and $P_F(\Omega)$ now available, we write the expressions for up and down transition distributions. These are

$$\beta_{\rm up}(\langle E\rangle, \Delta E, \theta) = I_0^{\rm up}(\Delta E, T, Z, N)[I_A(\Delta E, \lambda_1, E_1, \lambda_2, E_2)P_A(\Omega) + I_F(\Delta E, \lambda_3, E_3, \lambda_4, E_4)P_F(\Omega)] , \tag{5.3a}$$

and similarly for the down transitions,

$$\beta_{\rm down}(\langle E\rangle, \Delta E, \theta) = I_0^{\rm down}(\Delta E, T, Z, N)[I_A(\Delta E, \lambda_1, E_1, \lambda_2, E_2)P_A(\Omega) + I_F(\Delta E, \lambda_3, E_3, \lambda_4, E_4)P_F(\Omega)] , \tag{5.3b}$$

where I_0, I_A, and I_F are computed as in § 4.

6. NEUTRINO-NUCLEUS PROCESSES AND STELLAR COLLAPSE

None of the four neutrino-nucleus processes discussed here become important for supernovae until the core is well into the collapse epoch. As neutrinos begin to be trapped (for densities $\rho_{10} \geq 10$, where $\rho_{10} = \rho/10^{10}$ g cm^{-3}) each of the four neutrino processes contributes to the evolution of the neutrino distribution functions, as well as to the overall entropy, temperature, and lepton number histories of the infalling core. By far the dominant process in these considerations is endothermic scattering, since it is an up-transition with a great deal of weak strength. This process may be responsible for some lepton number loss before it shuts itself off at high density by filling up low-energy neutrino states (Kolb & Mazurek 1979). In any case all four processes taken together tend to compensate one another in their effects on the core properties. Nevertheless, detailed calculations of the evolution of the lepton distribution functions in the infalling core, post-bounce neutrino reheating of the material behind the stalled shock, or ν-induced nucleosynthesis will require the detailed fits to the processes which are provided in this paper.

It is useful to consider first the process of nuclear de-excitation into neutrino pairs. This discussion will serve to illustrate the level of accuracy of the fits described in the last section. This process is the dominant neutrino-pair energy-loss mechanism at high temperature in highly electron-degenerate environments. From equation (2.8a) we can derive that the total neutrino-pair energy-loss rate for a nucleus making a transition between discrete energy levels E_i and E_f is (Bahcall, Treiman, & Zee 1974),

$$\lambda_{if} \approx \frac{G^2 g_A^2}{60\pi^3}(E_i - E_f)^6 |M_{\rm GT}|^2 , \tag{6.1a}$$

where G is the weak coupling constant (nearly G_F), $g_A \approx 1.24$ is the ratio of axial-vector-to-vector coupling constants, and where, as above, we ignore the vector coupling. In this case $|M_{\rm GT}|^2$ is the Gamow-Teller matrix element. We find that

$$|M_{\rm GT}|^2 = \frac{j+1}{j}|\langle f|\boldsymbol{\sigma}\tau_3|i\rangle|^2 , \tag{6.1b}$$

where j is the spin of state i and where $|i\rangle$ and $|f\rangle$ represent the initial and final nuclear wave functions, respectively. An adequate approximation for the matrix element in equation (6.1a) is to take $|M_{\rm GT}|^2$ equal to that appropriate for charged-current beta decay (see eq. [17] in Fuller et al. 1982). The total energy-loss rate for a nucleus is then given by a sum over discrete nuclear transitions

$$\lambda = n_\nu \lambda_0 \sum_{if} |M_{\rm GT}|_{if}^2 (\Delta E_{if})^6 , \tag{6.1c}$$

where $n_\nu = 3$ is the number of neutrino flavors, $\lambda_0 = G^2 g_A^2/60\pi^3 \approx 1.74 \times 10^{-4}$ MeV^{-5} s^{-1}, and where $|M_{GT}|^2_{if}$ and ΔE_{if} are the matrix element and energy difference for transitions between states i and f. Consider the neutrino-pair energy-loss rate for the de-excitation of ^{56}Fe. In the zero-order shell model this nucleus would have two proton holes in the $1f_{7/2}$ shell and two neutrons in the $2p_{3/2}$ shell. It is clear that at relatively low temperature the dominant transitions would involve de-excitations between spin-orbit-partner levels which include $1f_{5/2}$–$1f_{7/2}$, $2p_{1/2}$–$2p_{3/2}$, and $1g_{7/2}$–$1g_{9/2}$ for both protons and neutrons. The probability of excitation of a neutron or proton to level i with spin j_i is (from eq. [3.7]),

$$n_i \approx (2j_i + 1)e^{-(\Delta E_{if}/T)}, \tag{6.2}$$

where ΔE_{if} is the energy difference between single particle levels, essentially the spin-orbit splitting. Technically these excitations correspond to the M1-excitations, and so the sum over spin-orbit partners indicated above would correspond closely to the M1 resonance for the ^{56}Fe ground state. Since these configurations represent particle-hole excitations the residual interaction will tend to collect strength and push it up in energy. We could include a positive particle-hole repulsion energy as in Fuller et al. (1982), but this has little effect on the rates, since the increase in the E^6 term is compensated by the decrease in the population index of the initial state. We can approximate the total energy-loss rate per ^{56}Fe nucleus by

$$\lambda_E \approx \lambda^p_{fp} + \lambda^p_{gd} + \lambda^n_{fp} + \lambda^n_{gd}, \tag{6.3a}$$

where λ^p_{fp} and λ^p_{gd} are the rates from proton excitations in the fp and gd shells, respectively, while the superscript n denotes the corresponding quantities for neutron excitations. Using equations (2.8a) and (3.1) we can write,

$$\lambda^p_{fp} = \lambda_0[|M_{ff}|^2 \times \tfrac{3}{8} \times 6 \times e^{-\Delta^p_{ff}/T}(\Delta^p_{ff})^6 + |M_{pp}|^2 \times 1 \times 2 \times e^{-\Delta^p_{pf}/T}(\Delta^p_{pp})^6], \tag{6.3b}$$

and similarly the neutron contributions are

$$\lambda^n_{fp} = \lambda_0[|M_{ff}|^2 \times \tfrac{1}{8} \times 6 \times e^{-\Delta^n_{ff}/T}(\Delta^n_{ff})^6 + |M_{pp}|^2 \times \tfrac{3}{4} \times 2 \times e^{-\Delta^n_{pp}/T}(\Delta^n_{pp})^6]. \tag{6.3c}$$

For the gd-shell transitions we can infer,

$$\lambda^p_{gd} = \lambda_0[|M_{gg}|^2 \times 1 \times 8 \times e^{-\Delta^p_{gg}/T}(\Delta^p_{gg})^6 + |M_{dd}|^2 \times 1 \times 4 \times e^{-\Delta^p_{dd}/T}(\Delta^p_{dd})^6], \tag{6.3d}$$

while similarly for the neutron transitions,

$$\lambda^n_{gd} = \lambda_0[|M_{gg}|^2 \times 1 \times 8 \times e^{-\Delta^n_{gg}/T}(\Delta^n_{gg})^6 + |M_{dd}|^2 \times 1 \times 4 \times e^{-\Delta^n_{dd}/T}(\Delta^n_{dd})^6], \tag{6.3e}$$

where $|M_{ff}|^2$ is the single particle Gamow-Teller matrix element for the $1f_{5/2}$–$1f_{7/2}$ transitions and similarly for $1p_{1/2}$–$1p_{3/2}$ (or pp), $2d_{3/2}$–$2d_{5/2}$ (or dd), and $1g_{7/2}$–$1g_{9/2}$ (or gg), and where, for example, Δ^p_{ff} is the proton single-particle excitation energy difference between $1f_{5/2}$ and $1f_{7/2}$, Δ^p_{pf} is that for $2p_{1/2}$–$1f_{7/2}$, while similarly Δ^p_{fg} is for $1f_{7/2}$–$1g_{7/2}$, while Δ^p_{fd} is for $2d_{3/2}$–$1f_{7/2}$, and Δ^p_{pp} is for $2p_{1/2}$–$2p_{3/2}$. The superscript n denotes the corresponding quantities for neutrons where, for example, Δ^n_{pg} is the $2p_{3/2}$–$1g_{7/2}$ splitting. All single-particle energies are the same as used in the numerical calculations in the previous sections and are listed through the gd-shell in Table 3.

For low temperatures ($T < 5$ MeV) it can be inferred from the above considerations that λ_{fp} is dominated by the $1f_{5/2}$–$1f_{7/2}$ transitions ($\Delta E \approx 6.5$ MeV) for both neutrons and protons, while λ_{gd} is dominated by the neutron $1g_{7/2}$–$1g_{9/2}$ transition ($\Delta E \approx 9$ MeV). A convenient fit to the neutrino-pair energy-loss rate (MeV s^{-1} nucleus^{-1}) using just these transitions for a nucleus of mass A is

$$\lambda_{fp} \approx (8.64 \times 10^5)\frac{e^{[-24.87/(TA^{1/3})]}}{A^2}, \tag{6.4a}$$

TABLE 3

SINGLE-PARTICLE ENERGIES FOR ^{56}Fe IN MeV

Shell	Neutrons	Protons
$1s_{1/2}$	−37.7195	−32.5067
$1p_{3/2}$	−30.5994	−24.9307
$1p_{1/2}$	−28.7018	−22.9301
$1d_{5/2}$	−22.7940	−16.6323
$2s_{1/2}$	−19.1850	−12.6992
$1d_{3/2}$	−18.7578	−12.2864
$1f_{7/2}$	−14.4634	−7.8884
$2p_{3/2}$	−10.2387	−3.5610
$2p_{1/2}$	−8.0895	−1.0365
$1f_{5/2}$	−7.9626	−0.7045
$1g_{9/2}$	−5.7389	1.0882
$2d_{5/2}$	−1.9587	4.4898
$3s_{1/2}$	−0.6869	5.6475
$2d_{3/2}$	1.0491	7.9622
$1g_{7/2}$	2.9483	10.8464
$1h_{11/2}$	3.2884	10.1549
$1h_{9/2}$	13.0656	20.9399

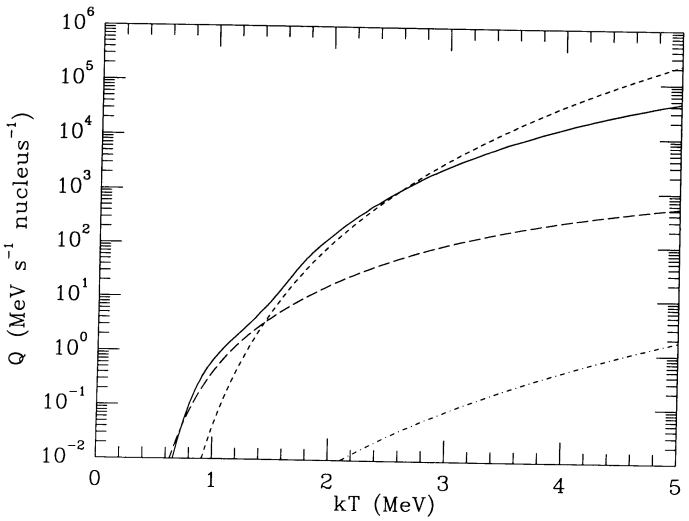

FIG. 7.—Energy-loss rates per nucleus as a function of temperature for ^{56}Fe as computed from eq. (2.8a) (*solid curve*), from eq. (6.4) (*long-dashed curve*), and from Kolb & Mazurek (1979) (*short-dashed curve*). The energy-loss rate per nucleon (divided by Y_e) from neutrino-pair bremsstrahlung is given as the dot-dashed curve.

and similarly for the *gd*-shell,

$$\lambda_{gd} \approx (2.40 \times 10^7) \frac{e^{[-53.83/(TA^{1/3})]}}{A^2}, \tag{6.4b}$$

where T is the temperature in MeV. We see immediately from this exercise that the energy scale which is important for determining the rates is not so much the temperature as the typical *spin-orbit splitting*. Schematically the nuclear energy-loss de-excitation rate scales as

$$\lambda \approx G_F^2 (\Delta E)^6 e^{-\Delta E/T}. \tag{6.5}$$

The ratio of the rates given by this expression for a transition energy $\Delta E \approx 7$ MeV (a typical spin-orbit energy difference) to a transition with energy $\Delta E \approx T$ if $T \approx 1.5$ MeV is of order 300. A strict Fermi gas treatment of the nucleus would miss this essential feature of the shell model.

We compare the energy-loss rates for ^{56}Fe (MeV s^{-1} nucleus^{-1}) for three different calculation techniques in Figure 7. The solid curve is the neutrino pair loss rate as calculated from equation (2.8a), with an integration of the detailed fit given in the last section. The long-dashed curve is the result from the simple schematic shell model discussed above (eq. [6.4a]). These curves track each other well at low temperature, as expected, where the *fp* and *gd* spin orbit transitions dominate. As the temperature increases, however, new channels open up and forbidden strength becomes important so that the result from equation (6.4) falls below the detailed fits. We show the independent single-particle model result (Fermi gas) of Kolb & Mazurek (1979) for comparison (*short dashed curve*). This model yields a rate which is below our result by one order of magnitude or more at low temperature ($T < 1.5$ MeV) where the *fp* and *gd* shell transitions dominate, but is considerably larger at high temperature where the Fermi gas technique overestimates the weak strength. Nevertheless, we concur with Kolb & Mazurek (1979) as to the effects of this process in stellar collapse. In fact this is the dominant neutrino-pair loss rate at high electron Fermi energy and temperature. To illustrate this we have plotted the energy-loss rate per nucleon (divided by electron fraction Y_e) from neutrino-pair bremsstrahlung (*dot-dashed curve*) as discussed in Dicus et al. (1976).

To gauge the relative importance of, and role of, the four neutrino-nucleus processes in stellar collapse we have performed some very simplistic one-zone collapse calculations. These are to be understood as illustrative of the relative role of the processes only, and are not intended to give the true evolution of entropy, temperature, composition, and the form of the lepton distribution functions in the infalling core. These quantities could be obtained only through a detailed multizone collapse code calculation with multi-energy-group ν-transport which could use our detailed numerical fits to the neutrino-nucleus rates. The overall equation of state and electron capture characteristics of our one-zone calculation are as described in Fuller (1982). However, we have modified this calculation at high densities to mock-up the effects of neutrino trapping and the consequent filling of neutrino phase space. Neutrinos begin to be trapped in the core at densities of the order of $\rho_{10} \approx 10$ when the neutrino diffusion time scales begin to become of order the dynamical time scale for collapse. The dominant neutrino opacity source here is conservative-coherent scattering on heavy nuclei. The highest energy neutrinos will be trapped first. Very crudely, the electron neutrino distribution function might resemble a Fermi-Dirac form with under filling (or a "window") at low energies (see Mayle 1985; Baron & Cooperstein 1990; Arnett 1977). If we idealize all neutrino states as being filled between the electron-neutrino Fermi energy, μ_ν, and a cutoff energy E_c (where E_c is the lowest neutrino energy that is trapped by the above criterion: the diffusive time scale for a neutrino of energy E_c, $\tau_{\rm dif}$, is equal to the dynamical time $\tau_{\rm grav}$), we can derive

$$E_c \approx (17 \text{ MeV}) \left(\frac{80}{A}\right)^{1/2} \left(\frac{30}{\rho_{10}}\right)^{5/12}, \tag{6.5}$$

where A is the mean nuclear mass number.

Neutrino phase space is filled up in these calculations by several processes, including electron capture on free protons and heavy nuclei, endothermic neutrino-nucleus scattering and nuclear de-excitation into neutrino pairs as well as neutrino-electron scattering. To estimate the rate at which the low-energy phase space is filled we first estimate the fraction of states below E_c which are occupied, f, in terms of the number of occupied neutrino states below E_c, n_ν, and the total number of states below E_c, n_ν^0. Thus we have,

$$f \approx \frac{n_\nu}{n_\nu^0}, \tag{6.6a}$$

where roughly,

$$n_\nu^0 \approx \frac{E_c^3}{6\pi^2}. \tag{6.6b}$$

The time evolution of n_ν can be estimated by

$$\frac{dn_\nu}{dt} \approx \lambda_p n_A - \frac{n_\nu}{\tau_{\rm dif}}, \tag{6.7}$$

Where λ_p is the rate at which neutrinos are downscattered into the window per nucleus and n_A is the number density of nuclei, and where $\tau_{\rm dif}$ is the neutrino diffusion time scale at the appropriate energy. The most important processes in this regard are electron capture, endothermic neutrino-nucleus scattering, and (at high temperature only) nuclear de-excitation into pairs. All of these processes are blocked in our calculation by $1-f$ at the appropriate energies for ν_e (note that nuclear de-excitation into ν_μ and ν_τ pairs remain unblocked).

The results of the one-zone calculations are shown in Figures 8, 9, and 10. In these figures entropy-per-baryon in units of Boltzmann's constant k, temperature and electron fraction are plotted versus ρ_{10} for three cases: complete blocking of all lepton-nucleus processes (*solid curve*), down-scattering of electron neutrinos and pair de-excitation of nuclei with no low-energy blocking (*short-dashed curve*), and down-scattering and pair de-excitation but with phase-space filling of low-energy ν_e phase space as described above (*long-dashed curve*). The calculation which would best track detailed collapse calculations is the complete blocking case. However, the other cases give insight into the gross effects of the neutrino-nucleus processes.

We have found that the entropy of the post-trapped core is little changed by nuclear de-excitation into pairs, since the temperature is so low $T \approx 1$ MeV. In fact, from equation (6.4) it can be shown that the entropy loss per baryon in units of Boltzmann's constant generated by this process is less than 0.01. This process will, however, produce most of the $\bar{\nu}_e$, and ν_μ and ν_τ pairs in the core. Endothermic scattering of ν_e quickly fills the low-energy window in our calculation. Were this window not filled quickly then electron capture could considerably heat the core and reduce the lepton number (here given by Y_e) and thus reduce the mass in the homologous core (see Bethe et al. 1979 and Burrows & Lattimer 1983). There may be some lepton number loss and concomitant entropy generation in the collapsing core due to endothermic scattering, but only a detailed collapse calculation using our fits will reveal how large this effect is.

Finally, we note that endothermic scattering may play a role in neutrino reheating of the stalled shock after core-bounce, in addition to the role it plays in nucleosynthesis. The reheating epoch begins about 0.15 s after bounce in the calculation of Mayle (1985) and Bethe & Wilson (1985) and is due primarily to ν_e and $\bar{\nu}_e$ absorption on free neutrons and protons. By contrast,

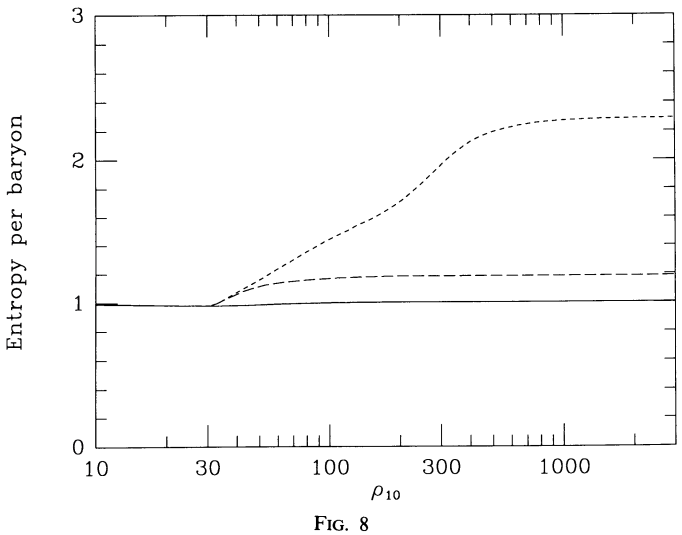

FIG. 8

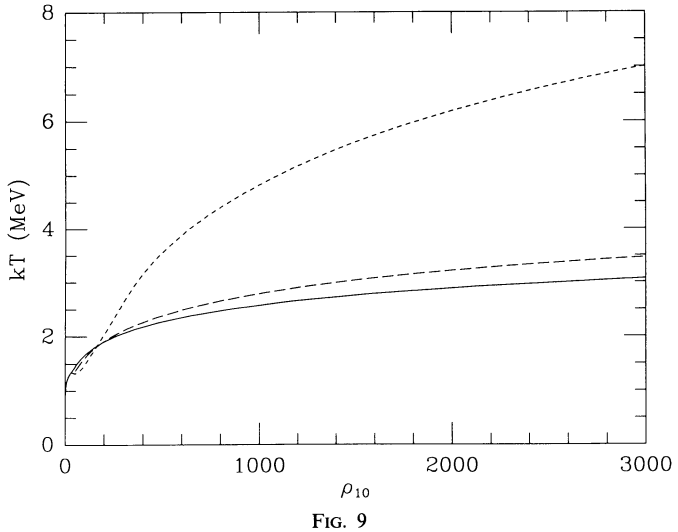

FIG. 9

FIG. 8.—Entropy per baryon as computed in one zone core collapse models. The quantity ρ_{10} is the density in units of 10^{10} g cm^{-3}. The models have either no neutrino-nucleus processes included (*solid curve*), down-scattering of electron neutrinos and pair de-excitation of nuclei (*short-dashed curve*), or down-scattering and pair de-excitation but with filling up of the low-energy window in the electron neutrino distribution (*long-dashed curve*).

FIG. 9.—Same as Fig. 8 but for temperature

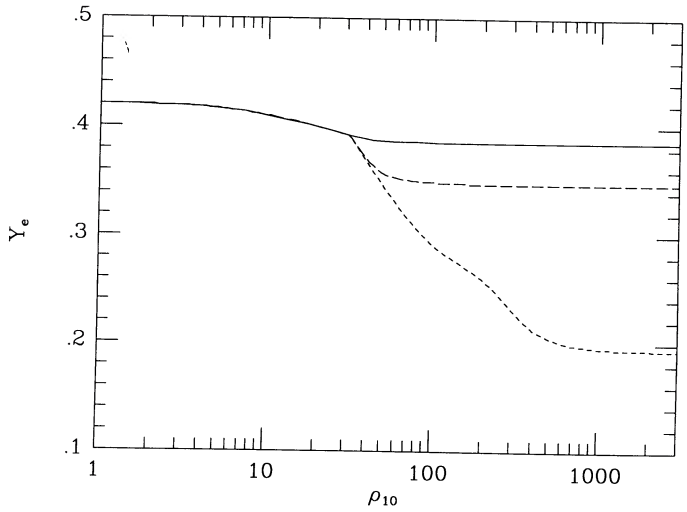

FIG. 10.—Same as Fig. 8 but for electron-to-baryon ratio Y_e

endothermic neutrino-nucleus scattering can tap into the higher energy (and higher luminosity) ν_μ and ν_τ neutrinos with scattering cross sections approaching 10^{-42} cm^2 per nucleon in heavy nuclei (at the beginning of reheating the entropy is still low enough that a substantial abundance of heavy nuclei exits), as discussed in Haxton (1988b).

In conclusion we have presented simple fitting formulae for our shell-model calculations of the rates of the four neutrino-nucleus processes in Figure 1. We have discussed the underlying nuclear physics of these processes in terms of the simple single-particle shell model. These processes may play an interesting role in the evolution of the lepton distribution functions in the infalling supernova core, the neutrino re-heating epoch of supernova, and the ν-process of nucleosynthesis.

The authors acknowledge very useful discussions with G. Brown, R. J. Gould, W. Haxton, J. R. Wilson, and (in 1979) E. W. Kolb. We wish to thank the hospitality of the Institute for Nuclear Theory at the University of Washington. This work was supported by NSF grant PHY-8914379 and IGPP grant LLNL 90-08 at UCSD and was performed under the auspices of the U.S. Department of Energy by the Lawrence Livermore National Laboratory under contract W-7405-ENG-48.

REFERENCES

Arnett, W. D. 1977, ApJ, 218, 815
Bahcall, J. N., Treiman, S. B., & Zee, A. 1974, Phys. Letters, 528, 275
Baron, E., & Cooperstein, J. 1990, ApJ, 353, 597
Bethe, H. A., Brown, G. E., Applegate, J., & Lattimer, J. M. 1979, Nucl. Phys., A324, 487
Bethe, H. A., & Wilson, J. R. 1985, ApJ, 295, 14
Bruenn, S., & Haxton, W. C. 1989, private communication
———. 1991, ApJ, submitted
Burrows, A., & Lattimer, J. M. 1983, ApJ, 270, 735
Dicus, D. A., Kolb, E. W., Schramm, D. N., & Tubbs, D. L. 1976, ApJ, 206, 481
Fuller, G. M. 1982, ApJ, 252, 741
Fuller, G. M., Fowler, W. A., & Newman, M. 1982, ApJ, 252, 715
Greuling, E., & Meeks, M. L. 1951, Phys. Rev., 82, 531
Haxton, W. C. 1987, Phys. Rev., D36, 2283
———. 1988a, Phys. Rev., C37, 2660
———. 1988b, Phys. Rev. Letters, 60, 1999
Kolb, E. W., & Mazurek, T. 1979, ApJ, 234, 1085
Mayle, R. 1985, Ph.D. thesis, UCRL-53713
Moretto, L. G. 1972, Nucl. Phys., A185, 145
Morita, M. 1953, Prog. Theor. Phys., 9, 345
Tubbs, D. L., & Koonin, S. 1979, ApJ, 232, L59
Woosley, S. E., Hartmann, D. H., Hoffman, R. D., & Haxton, W. C. 1990, ApJ, 356, 272
Woosley, S. E., Fowler, W. A., Holmes, J. A., & Zimmerman, B. A. 1978, Atomic Nucl. Data Tables, 23, 371